Catalysis Letters Vol. 112, Nos. 3–4, December 2006 (© 2006)
DOI: 10.1007/s10562-006-0193-9

Low-temperature water-gas shift reaction over Mn-promoted Cu/Al_2O_3 catalysts

Dinesh C. Yeragi, Narayan C. Pradhan, and Ajay K. Dalai*

Catalysis and Chemical Reaction Engineering Laboratories, Department of Chemical Engineering, University of Saskatchewan, S7N5A9 Saskatoon, SK, Canada

Received 19 July 2006; accepted 11 October 2006

Water-gas-shift reaction was carried our over a series of Mn-promoted Cu/Al_2O_3 catalysts in the temperature range of 448–533 K. The catalysts were characterized suitably by various techniques. The catalyst containing 8.55 wt% Mn was found to be the most active one among five catalysts tested. A maximum CO conversion of 90% was obtained over this catalyst at 513 K with a CO space-time of 5.33 h. The catalysts were found to be structure sensitive for the low-temperature water-gas shift reaction. A detailed kinetic study was performed for the reaction under investigation over the best catalyst. The kinetic data were fitted to two different models and the redox model was found to the better one than the other. From the estimated kinetic constant, the activation energy was determined to be 81 kJ/mol for the water-gas shift reaction in the temperature range of 448–463 K.

KEY WORDS: water–gas shift reaction; fuel cell; hydrogen production; Mn-promoted Cu/Al_2O_3 catalysts; kinetics; redox model.

1. Introduction

With the recent development and beginning of commercialization of polymer electrode fuel cells (PEFCs), the demand of CO-free hydrogen has increased to a great extent. In fact, development of a technology for the production of pure hydrogen (with little or no CO) conveniently and at a low cost is one of the challenges posed to the hydrogen-energy sector. Conventionally, water-gas shift (WGS) reaction, $CO + H_2O = CO_2 + H_2$, is applied in most hydrogen production facilities to decrease the concentration of CO (and to increase simultaneously the production of hydrogen). The shift reaction is desirable even for the removal of a large amount of CO since it is moderately exothermic ($\Delta H_{298} = -41.1$ kJ/mol) and the reaction temperature is easy to control. However, the equilibrium conversion of CO is dependent largely on the reaction temperature, lower temperature being favored for higher conversion of CO. Again the reactant gases are not active enough to reach the chemical equilibrium at lower temperatures. Copper-based catalysts are generally more active for WGS reaction. The present work is concerned with the development of manganese promoted Cu/Al_2O_3 catalysts for low-temperature water-gas shift reaction.

Generally, bimetallic catalyst systems are used for water-gas shift reaction. Two important industrial catalysts for water-gas shift reaction are: high-temperature shift catalyst, FeCr, and low-temperature shift catalyst CuZn [1]. Interestingly, copper-based catalysts are also used for methanol synthesis [2] and methanol steam reforming reactions [3,4], where the water-gas shift reaction plays an important role. Though copper-based catalysts have been the subject of extensive studies for the water-gas shift reaction ever since they were introduced in the early 1960s, some important aspects of the reaction over these catalysts have not yet been addressed properly. For example, the nature of active sites for copper-based shift catalysts is a topic of controversy. Some studies indicate that metallic copper is active for reaction [5], but the relative importance of metallic copper and Cu^{2+} sites is not clear.

The concept of structure sensitivity is widely used to describe the nature of catalytically active sites for the shift reaction. For structure sensitive catalysts, the specific activity (or the turnover frequency) of the reaction under consideration is strongly dependent on the catalyst parameters (e.g., catalyst composition, crystallite size distribution, nature of support, catalyst preparation parameters, etc. Lloyd *et al.* [1] had correlated the water-gas shift activity with the metallic copper surface area. According to them, the more the dispersion of metallic copper on the catalyst surface, the more active is the catalyst and a constant specific activity (or turnover frequency) is observed. Studies conducted by other researchers have also indicated that the turnover frequency is essentially constant over a wide range of metallic copper dispersions [6]. These studies seem to indicate that the catalyst parameters, like amount of copper dispersion, have no effect on the turnover frequency. Thus the water-gas shift reaction is structure insensitive on copper-based catalysts. On the other

*To whom correspondence should be addressed.
E-mail: ajay.dalai@usask.ca

hand, Kuijpers *et al.* [7] have proposed that the shift reaction is a structure sensitive reaction on silica supported copper catalysts, since the reaction takes place only on copper crystallites of size less than 20 nm.

The primary objective of this study was to develop Mn-promoted CuO/Al_2O_3 catalysts for low-temperature water-gas shift reaction. Catalyst characterization, experimental and kinetic studies were carried out on these catalysts to identify the active species, their role in the water-gas shift reaction activity and also to address the aforementioned points of controversy in the literature.

Although the WGS reaction involves only four small molecules, the reaction mechanism is quite complex. There are generally two reaction mechanisms proposed in the literature for the WGS reaction, associative and redox. In the first one, a formate species is formed which then decomposes to form CO_2 and H_2 [8–10]. On the other hand, the redox mechanism consists of a surface reduction ($H_2O + * \rightleftharpoons H_2 + O*$), followed by surface oxidation ($CO + O*\ CO_2 + *$). Some studies have predicted that the redox mechanism is prevalent [1,5,11–13]. Grenoble *et al.* [9] proposed a reaction sequence based on an associative mechanism including formic acid as an intermediate in order to account for the apparent bi-functionality of the supported catalyst systems. They concluded that the WGS reaction occurs in two sites with the metal activating carbon monoxide and the support sites as the principal sites for water activation. Salmi *et al.* [10] studied the low-temperature water-gas shift reaction on industrial CuO–ZnO catalysts at 473 and 523 K. They found that the power rate law expression changed when the temperature of reaction was varied, indicating the complex nature of the WGS reaction mechanism. A part of the present study was devoted to establish a suitable mechanism for the reaction under investigation over the developed catalyst.

2. Experimental

2.1. Materials

ACS grade copper nitrate trihydrate [$Cu(NO)_2{\cdot}3H_2O$] and manganese nitrate of 99.98% purity were obtained from Johnson Matthey Company, Ward Hill, MA, USA. Aluminum nitrate nonahydrate [$Al(NO_3)_3{\cdot}9H_2O$] and sodium carbonate, both of purity $>99.5\%$, were procured from BDH Chemicals Ltd., Toronto, ON, Canada.

2.2. Catalysts preparation

The catalyst was prepared in two major steps. In the first step, copper was loaded on alumina by co-precipitation technique from 105 g of a solution of copper nitrate trihydrate and aluminum nitrate nonahydrate having a copper/aluminum ratio of 0.52. Precipitation was brought about by adding this solution dropwise, with constant stirring, to 0.5 M sodium carbonate solution maintained at 40 °C in a 3 L flask. The quantity of sodium carbonate solution taken was 1.1 times the stoichiometric requirement. The resulting slurry (pH 7.5) was vigorously stirred for another 30 min. The precipitate was filtered and washed several times with warm water and finally with cold water and then dried at 383 K for 12 h in air. The dry coprecipitated precursor was designated as CA.

In the second step, the dried precipitate was pelletized in a hydraulic press under a compacting pressure of 680.5 atm, crushed and sieved into a pellet size ranging from −8 to +10 mesh (2.00–2.36 mm). These catalyst precursor pellets were then impregnated with manganese nitrate solutions having five different concentrations in the range of 0.2 to 2 M by an incipient wetness technique. The Mn-impregnated catalysts were dried first at 383 K for 12 h in an air oven and then calcined in a muffle furnace by raising the temperature slowly to 973 K and then keeping at this temperature for 3 h.

2.3. Catalyst characterization

The calcined promoted catalysts were characterized for various properties responsible for catalytic activity. The different techniques used for characterization include powder X-ray diffraction (XRD) with a Rogaku D/Max-RBX diffractometer (Rigaku, Tokyo, Japan), elemental analysis using inductively coupled plasma-atomic emission spectroscopy (ICP-AES) with a Thermo Jarrel Ash ICAP 61E Trace Analyzer (Thermo Instruments Canada Inc., Mississauga, ON, Canada), temperature programmed reduction (TPR) using ChemBET 3000 equipment (Quantachrome Corporation FL, USA), scanning electron microscopy (SEM) using Phillips SEM-505 scanning electron microscope, and BET surface area, pore volume and pore size distribution, low temperature oxygen chemisorption analysis using Micromeretics adsorption equipment (Model ASAP2000 manufactured by Micromeretics Instruments Inc., Norcross, GA, USA).

2.4. Experimental set-up and procedure

The experiments on water-gas shift reaction were carried out in a fixed-bed reactor set-up. A schematic diagram of the set-up is shown in figure 1. The reactor consisted of a stainless steel tube (10 mm id, 460 mm length) with a SS mesh placed at the center of the reactor to support the catalyst bed. The reactor was placed in an electrically heated furnace, the temperature of which was controlled by a Series SR22 microprocessor based auto tuning PID temperature controlled (Shimaden Co. Ltd., Tokyo, Japan).

The feed gas used for the experiments had a molar composition of 2% CO, 15% CO_2, 45% H_2 and 38% N_2 (obtained from Praxair, Mississauga, ON, Canada). A

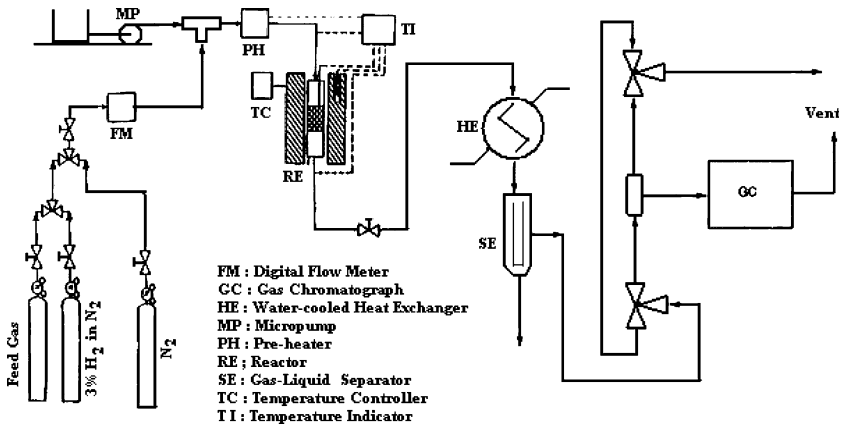

Figure 1. Schematic diagram of the experimental set-up.

digital mass flow meter was used to accurately measure the feed gas flow rate. A liquid metering pump was used to pump water. The feed gas and water were passed simultaneously in a pre-heater, which was set at a constant temperature of 523 K for all the experiments. The exit stream from the reactor was connected to a water-cooled condenser followed by an ice-cooled gas–liquid separator.

In a typical experiment, 2 g of one catalyst was mixed with 3 g of 1 mm diameter glass beads and placed in the fixed-bed reactor. Prior to experimentation, all catalysts were activated *in situ* by reducing at 573 K for 3 h in a stream of 3 mol% H_2 in N_2 (obtained from Praxair, Mississauga, On, Canada) flowing at 100 cm^3/min. After the desired reaction temperature was reached, the feed gas flow and the pump were started. After the steady state was achieved, the exit gas was collected in a gas sampler and analyzed for reaction products.

3. Results and discussion

3.1. Catalyst characterization

Elemental analysis. The elemental analysis of the calcined catalysts was performed using inductively coupled plasma atomic emission spectroscopy (ICP-AES). Table 1 shows the elemental compositions of five different Mn-promoted catalysts. As can be seen from this table, the copper concentration shows a monotonic decrease with addition of manganese. The elemental compositions are reported on a per unit catalyst weight basis. Therefore, with the increase in the Mn concentration from 1.8 to 10.9 wt%, the copper concentration decreases from 40.4 to 35.6 wt%.

X-ray diffraction studies. The X-ray diffraction (XRD) studies were performed on calcined promoted catalysts to identify the component phases. As can be seen from figure 2, XRD peaks at scanning angles characteristic of Cu_2O, CuO, $CuAl_2O_4$, Al_2O_3, $CuMnO_2$ and Mn_2O_3 species are present in the calcined catalyst. The copper hydroxycarbonate salts in the catalyst precursors are unstable at high calcination temperatures and decompose readily to the oxides of copper. $CuAl_2O_4$ species is formed as a result of the interaction between Al_2O_3 and CuO at high temperatures:. Likewise, the $CuMnO_2$ species is formed by the interaction between Cu_2O and Mn_2O_3:$Cu_2O + Mn_2O_3 \rightarrow 2CuMnO_2$. Mn_2O_3 is the stable oxide species of manganese resulting from the decomposition of the excess manganese hydroxide in the catalyst precursor at high temperature. As the promoter manganese concentration in the catalyst was increased, the peaks of $CuAl_2O_4$ and $CuMnO_2$ showed an increase in intensity, while the peak intensity of CuO dropped. Cu_2O, CuO and $CuAl_2O_4$ were also identified for copper catalysts by Idem and Bakhshi [14], and Robinson and Mol [15] using TPR and XRD characterization techniques.

Temperature programmed reduction. Figure 3 shows the temperature programmed reduction (TPR) profiles

Table 1
Physico-chemical properties of various catalysts

Catalyst Designation	Amount (wt%) of		BET surface area (m^2/g)	Total pore vol. (cm^3/g)	Avg. pore dia. (nm)
	Cu	Mn			
CA/M1	40.4	1.80	80.81	0.40	19.6
CA/M2	39.0	4.36	70.75	0.33	18.7
CA/M3	38.1	6.02	68.94	0.30	17.3
CA/M4	36.2	8.55	43.67	0.18	16.6
CA/M5	35.6	10.9	43.71	0.10	9.9

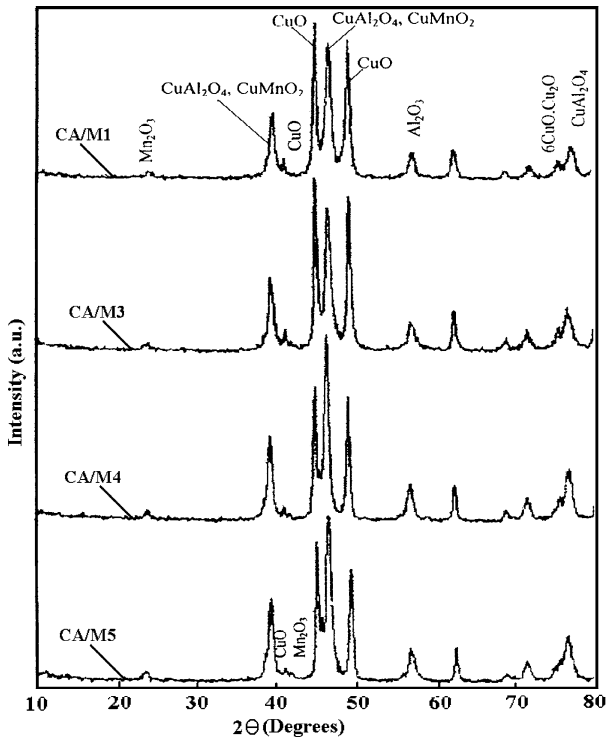

Figure 2. X-ray diffraction patterns of calcined Mn-promoted Cu/Al_2O_3 catalysts.

of Mn-promoted calcined catalyst. The peaks at ~473 K in the profile represent the reduction of Cu_2O. The presence of this species has been reported by Idem and Bakhshi [3]. The peaks at ca.548 K represent the reduction of CuO species. The oxides of copper are produced by thermal decomposition of copper hydroxide and copper hydrocarbonate species at high calcination temperatures. The wide peaks observed in the temperature range of ca.640–740 K represent the reduction of the species $CuAl_2O_4$ (formed as a result of the interaction between Al_2O_3 and CuO at high calcination temperature) The reduction peak of $CuMnO_2$ formed as a result of the interaction between the Cu_2O and Mn_2O_3 overlaps with the reduction peak of the $CuAl_2O_4$ species in the temperature range of ca.640–740 K. The $CuMnO_2$ and $CuAl_2O_4$ species also reduce to give metallic copper, but the copper formed is retained in the lattice structure and is not dispersed on the surface, like the copper crystallites formed by the reduction of Cu_2O and CuO. The TPR peak at ca. 833 K (see figure 3 for CA/M1) represents the reduction of Mn_2O_3, which is formed as a result of the decomposition of manganese hydroxide at high calcination temperatures.

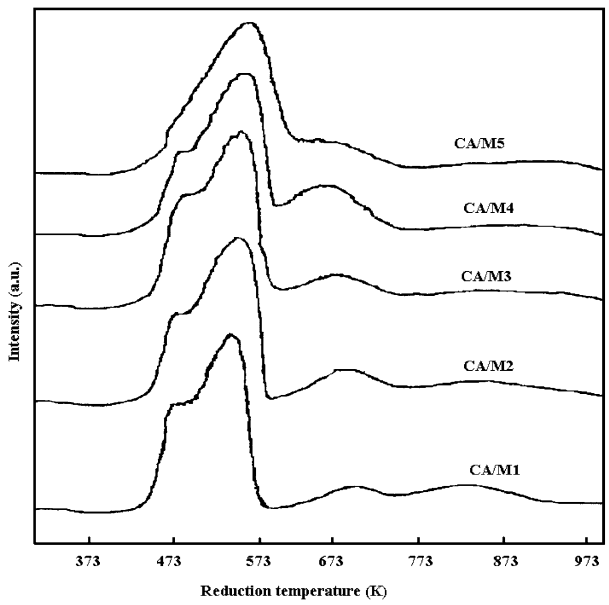

Figure 3. TPR profiles of calcined Mn-promoted Cu/Al_2O_3 catalysts.

The reduction temperature and the peak width are an indication of the ease of the reduction and the degree of interaction between the different species, respectively. High reduction temperature indicates difficulty in reduction and wide peak indicates a high degree of interaction between species. The peak area indicates the extent of reduction. As the Mn-promoter concentration in the catalyst increases, the combined peak for the reduction of $CuMnO_2$ and $CuAl_2O_4$ species shows a shift in the direction of lower temperature. The Cu_2O peak diminishes in intensity with increase in the promoter concentration. This indicates that as the promoter concentration increases, the interaction between the Cu_2O and Mn_2O_3 species also increases.

It is also seen from the TPR plots that as the Mn-promoter concentration increases, the reducibility of the CuO species decreases, i.e., temperature higher than 573 K is needed to completely reduce these species (see TPR profile of CA/M5 in figure 3). This is due to the interaction represented by the equation: $CuO + Al_2O_3 \rightarrow CuAl_2O_4$. This implies that when a reduction temperature of 573 K is used to activate the catalysts in the performance evaluation experiments, the active metallic copper surface area available decreases as the manganese promoter concentration increases (particularly so for the case of catalyst CA/M5).

Scanning electron microscopy. Scanning electron micrographs were taken for all calcined catalysts, both unreduced and reduced. Figure 4 shows the typical micrographs for catalyst CA/M3. In all cases, the reduced samples were found to possess smaller average particle size as compared to the corresponding unreduced samples. This is probably due to the reduction of the metallic oxide phases to their metallic states.

BET surface area, pore volume and pore size distribution. BET surface area, pore volume and pore size distribution studies were performed on the calcined catalyst and table 1 presents the results. The values of the surface area, average pore size and pore volume for

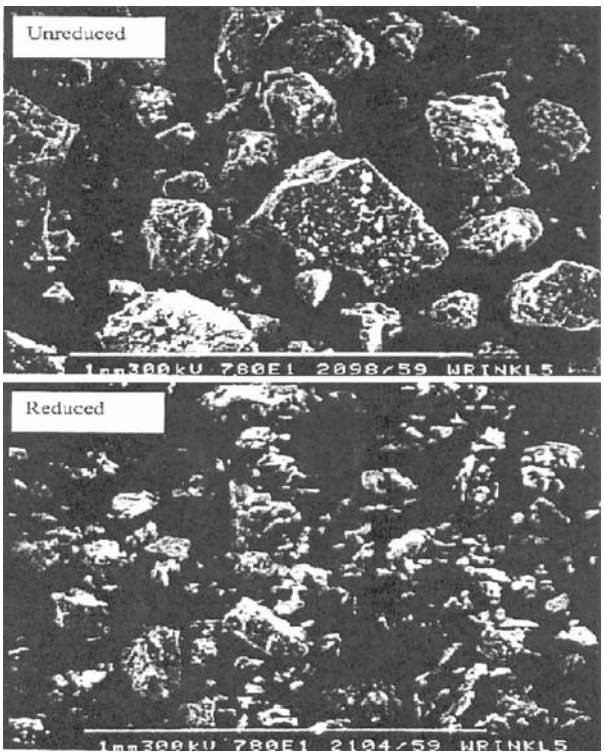

Figure 4. Scanning electron micrograph of unreduced and reduced CA/M3 catalyst.

the calcined catalysts decreased from 81 to 44 m^2/g, 19.6 to 9.6 nm and 0.4 to 0.1 cm^3/g, respectively, as the manganese concentration increased from 1.8 to 10.9 wt%. It can be seen from figure 5 that the pore size distribution of the calcined catalysts changed from monodisperse to bidisperse, as the manganese concentration was increased.

Low-temperature oxygen chemisorption. Low-temperature chemisorption analysis was performed to measure the copper surface area, copper dispersion and average copper crystallite size of the reduced catalysts. The surface area of copper was determined by oxygen chemisorption at the boiling point (78 K) of liquid nitrogen. At such low temperature, the chemisorption is not complicated by the bulk oxidation of the catalyst.

As the Mn promoter concentration was increased from 1.79 to 8.55 wt%, the copper dispersion and copper surface area decreased from 11.8 to 8.94%, and from 30.74 to 20.86 m^2/g, respectively. The metallic copper is obtained by the reduction of Cu_2O and CuO species at 573 K. At high calcination temperatures, it is known that the Cu_2O species interact with Mn_2O_3 to form $CuMnO_2$ and CuO with Al_2O_3 to form $CuAl_2O_4$ as discussed earlier. From the TPR plots, it was observed that the $CuMnO_2$ and $CuAl_2O_4$ species had a reduction temperature in the range of 640–740 K. Therefore, these species do not reduce with hydrogen to form metallic copper at a reduction temperature of 573 K. Thus some of the copper is retained in the $CuMnO_2$ and $CuAl_2O_4$ species. With an increase in the Mn promoter concentration, the interaction between Cu_2O and Mn_2O_3 to form $CuMnO_2$ and between CuO and Al_2O_3 to form $CuAl_2O_4$, increased. This resulted in a drop in the copper surface area and copper dispersion.

3.2. Catalyst performance evaluation

The various prepared catalysts were screened for their activity towards water-gas shift reaction in the microreactor under otherwise identical conditions. The catalyst activity was evaluated in terms of CO conversion for the water-gas shift reaction. A few data points were repeated to check the reproducibility of the results. The uncertainty of the experimental results was found to lie within 1–2%. The water-gas shift activity of each catalyst was expressed in terms of the percentage of CO converted using the following equation:

$$X_{CO} = \frac{Y_{CO_{in}} - Y_{CO_{out}}}{Y_{CO_{in}}} \times 100$$

where $Y_{CO_{in}}$ and $Y_{CO_{out}}$ are the number of moles of carbon monoxide in the reactor feed and the reactor effluent, respectively. The data obtained from the CO_2 and H_2 measurements were used to crosscheck the CO conversion as calculated from the CO concentration using the above formula. A satisfactory carbon balance (>98%) was obtained for the reaction points thus indicating that there was no carbon deposition on the catalyst or on the reactor walls.

Effect of promoter Mn concentration. Experiments were carried out with all five different catalysts having varying Mn content in the range of 1.8–10.9 wt%. Figure 6 shows the CO conversions obtained at different Mn loadings for two temperatures. As can be seen from this figure, the CO conversion increases first with Mn concentration in the catalyst reaches a maximum at 8.55 wt% loading (with catalyst CA/M4) and then decreases for higher loadings of Mn. The decrease is CO conversion may be due to the drop in copper surface area at higher copper loadings as reported earlier.

Effect of space-time. Experiments were performed to study the effect of space-time on the conversion of CO using different catalysts. Figure 7 shows the CO conversions obtained with different catalysts at various W/F_{CO} ratios ranging from 2.5 to 16 h at a temperature of 513 K (dry GHSV ranging from 9600 to 1600 h^{-1}). As was expected, the CO conversion increased as the feed contact time was increased. Beyond a W/F_{CO} ratio of 6 h, the CO conversion did not show a significant increase and a plateau was reached. A maximum CO conversion of 90 mol% was obtained at 513 K and W/F_{CO} ratio of 5.33 h for the catalyst CA/M4 containing 8.5 wt% Mn.

While copper metal is the active species for the water-gas shift reaction, it should be noted that it is not the only species that is taking part in the reaction. The

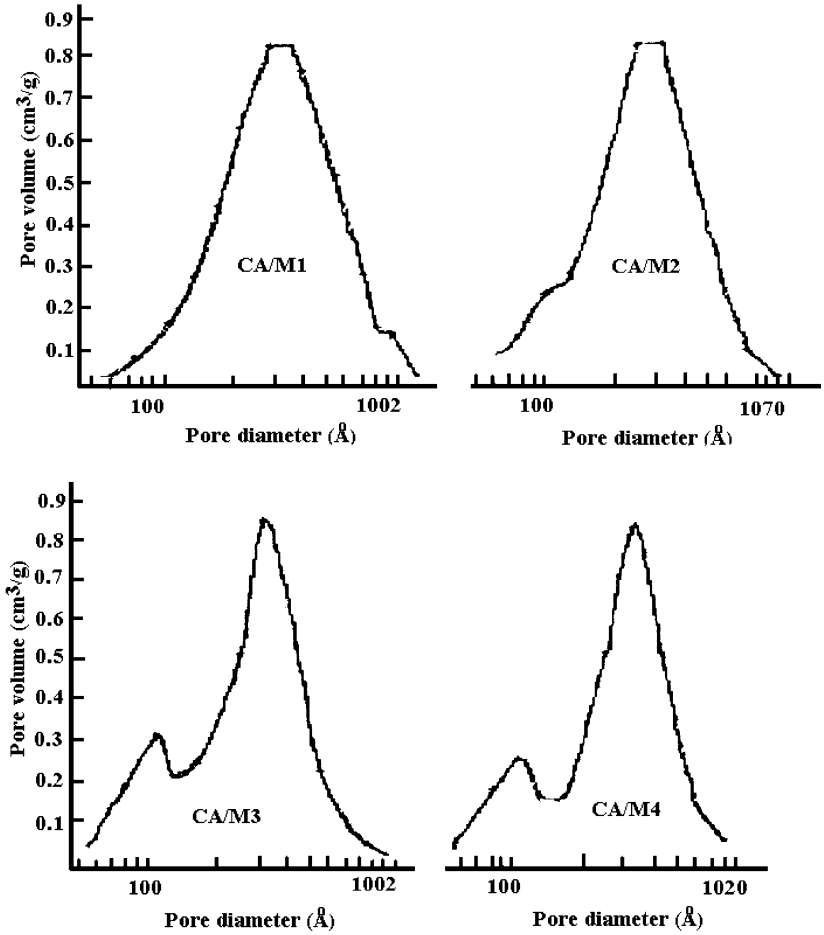

Figure 5. Pore size distribution of calcined Mn-promoted Cu/Al_2O_3 catalysts.

catalysts with low promoter concentrations showed a higher copper dispersion and metal copper surface area. But these catalysts were less active as compared to the catalysts containing higher concentrations of Mn. As the promoter concentration was increased, the result was the formation of species like $CuMnO_2$, which had low reducibility. Thus, in the case of the promoted catalysts, the role of Mn species is to keep the copper in the non-zero oxidation state. The presence of these species around the active copper metal increases the electron accepting potential of the catalyst. The water-gas shift reaction can be considered as an oxidation-reduction reaction with CO oxidized by a net loss of electrons and steam reduced by a net gain of electrons. The catalytic activity will be at its maximum if the electron accepting potential of the active sites increases.

But it was also seen from the TPR plots that with a further increase in the Mn-promoter concentration (10.9 wt%), the reducibility of the CuO species decreased, i.e., temperature greater then 573 K was needed to completely reduce these species to copper (see figure 3 for CA/M5). For the case of catalyst CA/M5 (10.9 wt% Mn), this implied that when a reduction temperature of 573 K was used to activate the catalyst in the performance evaluation experiments, the active metallic copper surface area available for reaction decreased drastically. Hence the activity of the catalyst dropped down. Thus the catalyst activity is maximum for an optimum ratio of metallic copper and copper in the non-zero oxidation state. This optimum ratio was achieved for the catalyst CA/M4 as could be seen from turnover frequency plots.

The turnover frequencies (TOF) (s^{-1}) for various Mn-promoted Cu/Al_2O_3 catalysts were determined and plotted as a function of temperature (figure 8). As can be seen from figure 8, the TOF of the catalysts increases with increase in temperature, reaches a maximum at 513 K and then decreases slightly for temperatures above 513 K. Moreover, at a particular temperature, catalyst CA/M4 having 8.55 wt% Mn was found to have maximum TOF.

Figure 9, shows the TOF as a function of CO space-time (W/F_{CO}) for the Mn-promoted catalysts at 513 K. For all the catalysts, the turnover frequencies were found to decrease with increase in the W/F_{CO} ratio. At a particular W/F_{CO} ratio, the TOF increases with increase

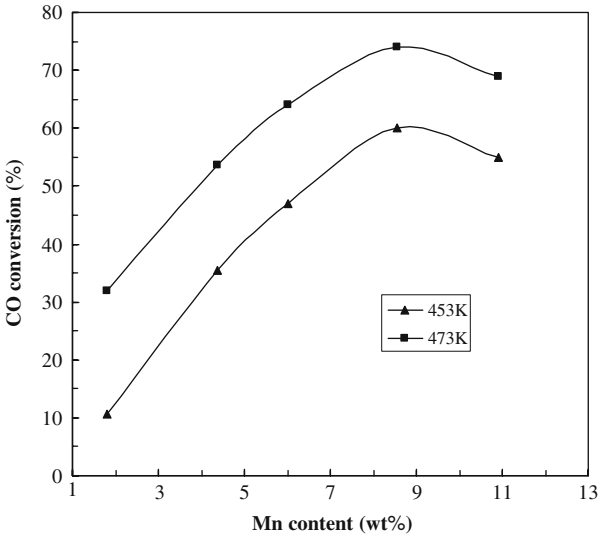

Figure 6. Effect of manganese concentration on CO conversion.

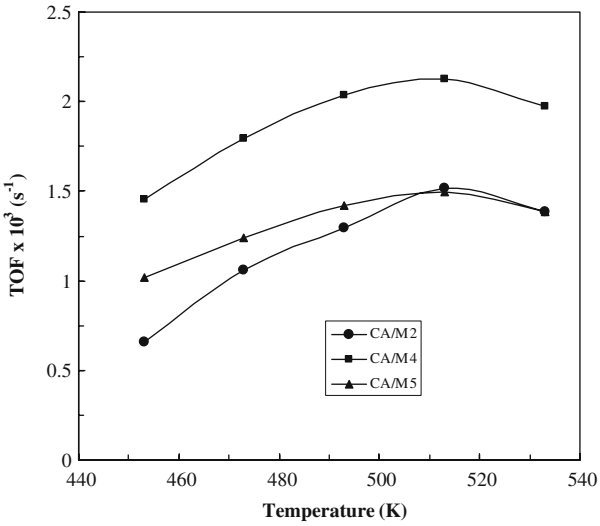

Figure 8. Variation of turnover frequency with temperature.

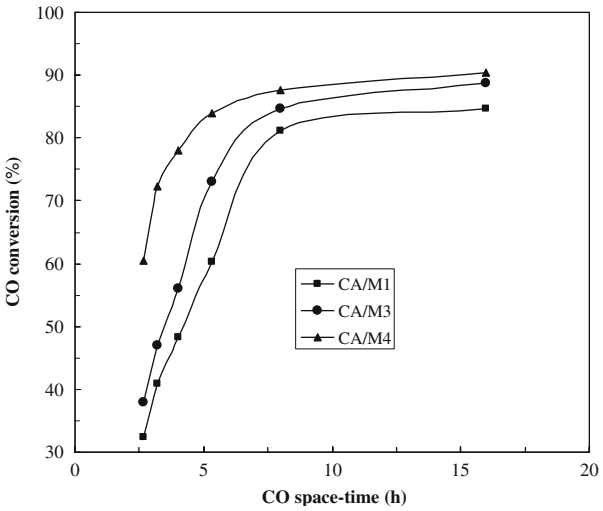

Figure 7. Effect of space-time on CO conversion.

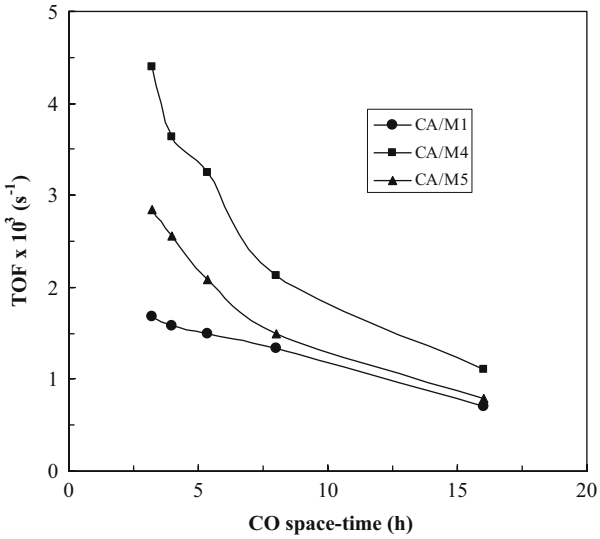

Figure 9. Variation of turnover frequency with CO space-time.

in Mn concentration from 1.8 to 8.55 wt%. The catalyst CA/M4 again showed the highest value of TOF. With further increase in promoter (Mn) concentration in the catalyst from 8.55 to 10.9 wt%, the TOF value showed a drop.

From the foregoing discussion on catalyst characterization and performance studies, it can be inferred that the dispersion of the catalytically active copper metal has no significant effect on the CO conversion (figure 10). The highly active catalysts are the ones with comparative lower copper dispersion and copper metal surface areas, as indicated by the turnover frequency plots. The Mn-promoted Cu/Al_2O_3 catalysts are thus structure sensitive for the low-temperature water-gas shift reaction.

3.3. Mass transfer consideration

The water-gas shift reaction on copper based catalysts is kinetically active even at low temperatures. Therefore, the reaction system may suffer from mass transfer limitations. However, for any kinetic study, the reaction system should be free from mass transfer resistances. For gas–solid reactions, this resistance can be either external or internal, within the catalyst pellets.

Elimination of external mass transfer resistance. Experiments were carried out with three different catalyst (CA/M3) loadings of 1, 2 and 3 g, respectively. In all three cases, the catalyst pellets were mixed with glass beads (0.5 mm) such that the ratio $L_b/d_p > 40$, where L_b is the bed height and d_p is the diameter of the catalyst pellet. This ensured that there was no channeling and

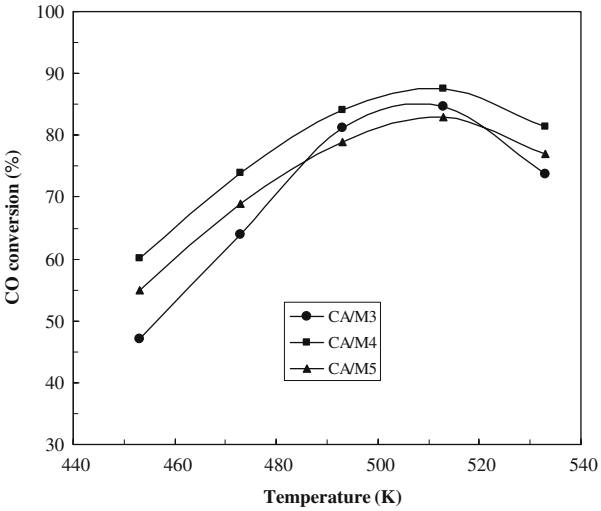

Figure 10. Effect of temperature on CO conversion.

the flow was close to plug flow. The feed gas flow was adjusted in such a way that the W/F_{CO} ratio remained same for all catalyst loadings. The results shown in table 2 indicate that the conversions of CO for all three catalyst loadings at constant W/F are independent of feed rates. Therefore, the external mass transfer resistance is negligible.

Elimination of internal mass transfer resistance. Experiments were also conducted to test the intraparticle diffusional limitations by varying the catalyst particle size while keeping space-time (for CO) constant. The experimental data obtained are presented in table 3. The results showed that there was almost no change in conversion of CO with catalyst size indicating negligible intraparticle mass transfer resistance in the particle size range studied. The particle sizes employed in the kinetic study were within the intraparticle diffusion free range.

The Thiele modulus was also calculated at the reaction conditions used for catalyst's performance evaluation experiments. The reaction rate model used for this calculation was the power law model developed from the kinetic studies with the catalyst CA/M4. From the value of the Thiele modulus of approximately unity, it was further confirmed that the intraparticle diffusional limitations were absent within the catalyst pellet and the surface reaction was the rate controlling step.

Table 2
Effect of external diffusional resistances on conversion of CO

Temperature (K)	Conversion of CO (%) with a superficial gas velocity (m/s) of		
	3.12[a]	6.25[b]	9.35[c]
453	41.72	46.92	44.27
473	59.82	63.94	60.92
493	73.75	81.16	80.74

Conditions: W/F_{CO}, 8.0 h; catalyst, CA/M3; average catalyst size, 0.5 mm; [a]1.0 g catalyst; [b]2 g catalyst; [c]3 g catalyst.

Table 3
Effect of intraparticle diffusion on conversion of CO

Particle size(mm)	Conversion of CO (%) with a CO space-time (h) of		
	4.5	8.0	13.5
0.5	64.2	84.7	90.0
1.0	64.0	83.5	89.3

Conditions: Temperature, 513 K; catalyst, CA/M3; catalyst loading, 2 g.

3.4. Kinetic modeling

Kinetic experiments were carried out by operating the reactor in the differential mode (5–10% conversion of CO) so that the gas composition, pressure and temperature were uniform throughout the reactor. The gas flow rates used during kinetic runs were much higher (lower space-time) than that used before to test for external mass transfer resistance. The high gas velocity further ensured that the film resistance to external mass transfer was absent during kinetic runs. Lower temperature region was preferred as the surface reaction would be slower compared to mass transfer thereby ensuring further the surface reaction as the controlling step.

The kinetic runs were taken under operating conditions free from mass transfer resistance at four different temperatures, namely 448, 463, 478 and 493 K. The catalyst CA/M4 was used for kinetic study as it showed highest activity during performance evaluation. For each temperature, the space-time-conversion data were analyzed and the rates of reaction were obtained by differential analysis of the plug flow reactor equation:

$$-r_{obs} = \frac{dX_{CO}}{d(W/F_{CO})}$$

Langmuir–Hishelwood model. Expression for the rate of reaction of CO was derived following Langmuir–Hinshelwood approach. The following associative mechanism was considered for developing the rate equation.

$$CO\ (g) + (*) \rightleftharpoons CO_{ads} \quad (1)$$

$$CO_{ads} + H_2O\ (g) \rightleftharpoons HCOOH_{ads} \quad (2)$$

$$HCOOH_{ads} \rightleftharpoons H_{2\,ads} + CO_2(g) \quad (3)$$

$$H_{2\,ads} \rightleftharpoons H_2(g) + (*) \quad (4)$$

Van Hewijnen and de Jong [8] proposed that the decomposition of the adsorbed formate on the surface is the rate determining step. Therefore, reaction steps (1), (2) and (4) are in equilibrium. Accordingly, the following expression was derived for the rate of reaction of CO:

$$-r_{CO} = \frac{k_3 K_1 K_2 p_{CO} p_{H_2O}}{1 + K_1 p_{CO} + K_1 K_2 p_{CO} p_{H_2O} + \frac{p_{H_2}}{K_4}} (1 - \beta) \quad (5)$$

where β is the reversibility factor for the water-gas shift reaction, given by

$$\beta = \frac{p_{H_2}\, p_{CO_2}}{(K_1\, K_2\, K_3\, K_4)\, p_{CO}\, p_{H_2O}} = \frac{p_{H_2}\, p_{CO_2}}{K\, p_{CO}\, p_{H_2O}} \quad (6)$$

The experimental data were fitted to equation (5) using Marquardt non-linear regression algorithm [16]. Table 4 gives the values of the kinetic constant (k_3) of controlling reaction (3) estimated at different temperatures. Figure 11 shows the Arrhenius plot for the variation of this rate constant with temperature. As can be seen from this figure, the line has got two different slopes for different temperature ranges. From the slopes of the line segments, the activation energies were determined as 344 and 83.5 kJ/mol for high- and low-temperature ranges, respectively. As it is not a proper trend, the model was rejected for the catalyst system under investigation.

Table 4
Estimated kinetic constants from various models

Temperature (K)	k_3 (L–H model) (gmol $gcat^{-1}$ h^{-1})	k_2 (Redox model) (gmol $gcat^{-1}$ h^{-1} atm^{-1})
448	0.017	0.0217
463	0.033	0.0437
478	0.092	0.0480
493	0.223	0.0518

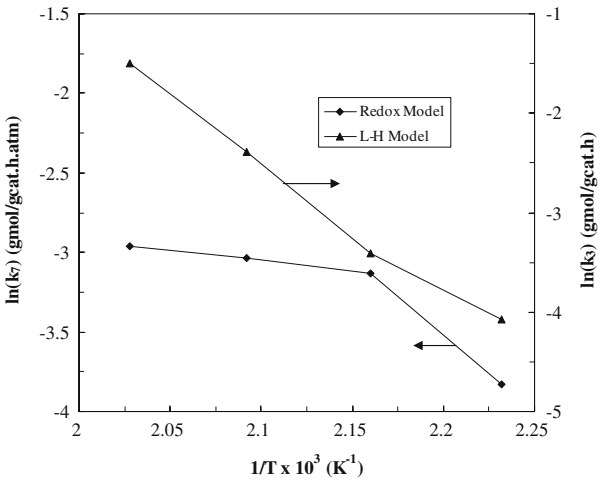

Figure 11. Arrhenius plots for various models.

Oxidation-Reduction (Redox) model. The oxidation reduction (or Redox) mechanism for water-gas shift reaction as proposed by Kuijpers et al. [7] is shown below:

$$H_2O\ (g) + (*) \rightleftharpoons H_2(g) + O_{ads} \quad (7)$$

$$CO\ (g) + O_{ads} \rightleftharpoons CO_2(g) + (*) \quad (8)$$

This regenerative mechanism for the water-gas shift reaction has been validated with experimental results by Chinchen et al. [2] and Gines et al. [6]. The reaction step represented by equation (7) is considered to be the rate determining step so that the other reaction may be considered at equilibrium. Accordingly, the rate of reaction of CO was derived as

$$-r_{CO} = \frac{k_7\, p_{H_2O}}{1 + \frac{p_{CO_2}}{K_8\, p_{CO}}} (1 - \beta) \quad (9)$$

where

$$\beta = \frac{p_{H_2}\, p_{CO_2}}{(K_7\, K_8)\, p_{CO}\, p_{H_2O}} = \frac{p_{H_2}\, p_{CO_2}}{K'\, p_{CO}\, p_{H_2O}} \quad (10)$$

The reaction rate data were fitted to the oxidation reduction model equation (9) following the same procedure as earlier with the formate model. The kinetic constant (k_7) estimated at different temperatures by best-fit is presented in table 4. An Arrhenius plot of the rate constant (k_7) for the rate determining step is also shown in figure 11. Two distinct activation energy regions were observed in this plot as well. At lower temperatures, an activation energy of 81 kJ/mol was obtained. Koryabkina et al. [13] have reported an activation energy value of 62 kJ/mol for WGS reaction over CuO/Al_2O_3 at 473 K and a value of 79 kJ/mol over $CuO–ZnO/Al_2O_3$ at 463 K.

For the high temperature region, an activation energy value of 11 kJ/mol was obtained. At higher temperatures, the diffusional resistances become predominant leading to a reduction in the activation energy as observed. As the redox model could predict proper trend in activation energy, it is most suitable for the present catalyst system for water-gas shift reaction.

4. Conclusions

Low-temperature water-gas shift reaction was carried out over several Mn-promoted Cu/Al_2O_3 catalysts. The catalysts were characterized for their properties relevant to the reaction under consideration. The catalyst containing 8.55 wt% Mn showed highest activity. It was having a copper dispersion of 8.95 wt% and a copper metal surface area of 20.86 m^2/g. The Mn-promoted Cu/Al_2O_3 catalysts were found to be structure sensitive for the low-temperature water-gas shift reaction.

A detailed kinetic study was performed over the most active catalyst under suitable experimental conditions ensuring no mass transfer resistance in the reaction system. Two different kinetic models, namely Langmuir–Hinshelwood type associative model and redox model were followed and respective model equations were formulated. Kinetic data were fitted to the models and the redox model was found to be most suitable in representing the waster–gas shift reaction over the developed catalyst.

References

[1] L. Lloyd, D.E. Ridler and M.V. Twigg, The water-gas shift reaction, Pages 283–338 in: *Catalyst Handbook*, M.V. Twigg (eds.), 2 ed.(Wolfe Publishing, Frome, 1989) pp. 283–338.
[2] G.C. Chinchen, M.S. Spencer, K.C. Waugh and D.A. Whan, J. Chem. Soc. Faraday Trans. I83 (1987) 2193.
[3] R.O. Idem and N.N. Bakhshi, Ind. Eng. Chem. Res. 33 (1994) 2047.
[4] R.O. Idem and N.N. Bakhshi, Ind. Eng. Chem. Res. 33 (1994) 2056.
[5] J. Nakamura, J.M. Campbell and C.T. Campbell, J. Chem. Soc. Faraday Trans. 86 (1990) 2725.
[6] M.J.L. Gines, N. Amadeo, M. Laborde and C.R. Apesteguia, Appl. Catal. A Gen. 131 (1995) 283.
[7] E.G.M. Kuijpers, R.B. Tjepkema and W.J.J. Vander Wall, Appl. Catal. 25 (1986) 139.
[8] T. Van Herwijnen and W.A. De Jong, J. Catal. 63 (1980) 83.
[9] D.C. Grenoble, M.M. Estadt and D.F. Ollis, J. Catal. 67 (1981) 90.
[10] T. Salmi and R. Hakkarainen, Appl. Catal. 49 (1989) 285.
[11] C.V. Ovesen, P. Stoltze, J.K. Nørskov and C.T. Campbell, J. Catal. 134 (1992) 445.
[12] C.V. Ovesen, B.S. Clausen, B.S. Hammershoei, G. Steffensen, T. Askgaard, I. Chorkendorff, J.K. Nørskov, P.B. Rasmussen, P. Stoltze and P. Taylor, J. Catal. 158 (1996) 170.
[13] N.A. Koryabkina, A.A. Phatak, W.F. Ruettinger, R.J. Farrauto and F.H. Ribeiro, J. Catal. 217 (2003) 233.
[14] R.O. Idem and N.N. Bakhshi, Can. J. Chem. Eng. 74 (1996) 288.
[15] W.R.A.M. Robinson and J.C. Mol, Appl. Catal. 44 (1988) 165.
[16] D.W. Marquardt, J. Soc. Indtl. Appl. Math. 11 (1963) 431.